Journal of Geophysical Research: Oceans

RESEARCH ARTICLE
10.1029/2018JC014187

Coastal Upwelling Revisited: Ekman, Bakun, and Improved Upwelling Indices for the U.S. West Coast

Michael G. Jacox[1,2], Christopher A. Edwards[3], Elliott L. Hazen[1], and Steven J. Bograd[1]

[1]NOAA Southwest Fisheries Science Center, Monterey, CA, USA, [2]NOAA Earth System Research Laboratory, Boulder, CO, USA, [3]University of California, Santa Cruz, CA, USA

Key Points:
- New upwelling indices are presented for the U.S. West Coast (31–47°N) to address shortcomings in historical indices
- The Coastal Upwelling Transport Index (CUTI) estimates vertical volume transport (i.e., upwelling/downwelling)
- The Biologically Effective Upwelling Transport Index (BEUTI) estimates vertical nitrate flux

Supporting Information:
- Supporting Information S1

Correspondence to:
M. G. Jacox,
michael.jacox@noaa.gov

Citation:
Jacox, M. G., Edwards, C. A., Hazen, E. L., & Bograd, S. J. (2018). Coastal upwelling revisited: Ekman, Bakun, and improved upwelling indices for the U.S. West Coast. *Journal of Geophysical Research: Oceans*, *123*. https://doi.org/10.1029/2018JC014187

Received 18 MAY 2018
Accepted 26 SEP 2018
Accepted article online 2 OCT 2018

Abstract Coastal upwelling is responsible for thriving marine ecosystems and fisheries that are disproportionately productive relative to their surface area, particularly in the world's major eastern boundary upwelling systems. Along oceanic eastern boundaries, equatorward wind stress and the Earth's rotation combine to drive a near-surface layer of water offshore, a process called *Ekman transport*. Similarly, positive wind stress curl drives divergence in the surface Ekman layer and consequently upwelling from below, a process known as *Ekman suction*. In both cases, displaced water is replaced by upwelling of relatively nutrient-rich water from below, which stimulates the growth of microscopic phytoplankton that form the base of the marine food web. Ekman theory is foundational and underlies the calculation of upwelling indices such as the "Bakun Index" that are ubiquitous in eastern boundary upwelling system studies. While generally valuable first-order descriptions, these indices and their underlying theory provide an incomplete picture of coastal upwelling. Here we review the relevant dynamics and limitations of classical upwelling indices, particularly related to representation of the surface wind stress, the influence of geostrophic currents, and the properties of upwelled water. To address these shortcomings, we present two new upwelling indices for the U.S. West Coast (31–47°N), which are available from 1988 to present. The Coastal Upwelling Transport Index and the Biologically Effective Upwelling Transport Index provide improved estimates of vertical transport and vertical nitrate flux, respectively, by leveraging technological and scientific advances realized since the introduction of the Bakun Index nearly a half century ago.

Plain Language Summary The California Current System, running along the North American West Coast, hosts a rich and diverse marine ecosystem that provides considerable socioeconomic benefit. The process underlying this exceptional biological productivity is wind-driven coastal upwelling, which delivers deep, nutrient-rich water to the sunlit surface layer and stimulates growth of phytoplankton that form the base of the marine food web. Given the ecological importance of upwelling, indices designed to monitor its intensity (e.g., the "Bakun Index") were introduced nearly 50 years ago. While these indices have proved extremely useful, they have a number of limitations as they are derived from relatively coarse resolution atmospheric pressure fields. In particular, uncertainties arise in the estimation of wind stress and from the omission of the influence of ocean circulation. Furthermore, historical indices estimate only the amount of water upwelled, not the nutrient content of that water. Here we present new indices that leverage ocean models, satellite data, and in situ observations to more accurately estimate upwelling strength as well as the amount of nitrate being upwelled. The new indices are publicly available, extend from 1988 to present, and will be valuable for monitoring upwelling in near real time and for understanding its impacts on the marine ecosystem.

1. Introduction

Wind-driven coastal upwelling is a key driver of physical, biogeochemical, and ecological variability near the land-sea interface, particularly in eastern boundary upwelling systems (EBUSs), which are characterized by seasonal equatorward wind forcing. Nutrient-rich water, supplied to the sunlit surface layer by wind-driven upwelling, stimulates the growth of phytoplankton that ultimately fuel diverse and productive marine ecosystems. In addition to this bottom-up forcing through the base of the food web, upwelling can influence higher trophic levels directly through exposure to physical and chemical signatures of the deeper ocean (e.g., lower temperature, oxygen concentration, and pH). Impacts of upwelling variability can be felt on timescales ranging from single events (days) to decades and longer, and they propagate to commercial and recreational activities that derive considerable socioeconomic benefit from EBUSs (Bograd et al., 2016). It is no surprise

then that these regions, and the coastal upwelling that underlies their functioning, garner significant attention from the oceanographic community.

The dynamics of wind-driven coastal upwelling were first described mathematically by V. Wilfrid Ekman (Ekman, 1905), who was invited to work on the problem by explorer and scientist Fridtjof Nansen. Nansen had observed on his Arctic expedition that sea ice drifted 20–40° to the right of the prevailing wind (Nansen, 1902) and explained the phenomenon as a consequence of the interaction between frictional forces (surface wind) and the rotation of the earth, an explanation confirmed by Ekman's theory. More than a century after its introduction, Ekman theory stands as foundational dynamical oceanography and the basis for our understanding of wind-driven ocean circulation.

Given the importance of coastal upwelling as a driver of EBUS dynamics, the utility of quantifying its variability in space and time was recognized decades ago. However, the spatiotemporal variability of oceanic vertical velocities and their weak signal relative to horizontal velocities prohibit direct monitoring of upwelling. To address the need for historical and continuous estimates of coastal upwelling intensity, Andrew Bakun (1973, 1975) developed the National Oceanic and Atmospheric Administration's (NOAA's) coastal upwelling index (Schwing et al., 1996), commonly referred to as the *Bakun Index*. The Bakun Index uses available estimates of atmospheric conditions and Ekman theory to derive estimates of cross-shore Ekman transport as a proxy for coastal upwelling. Over the past 40+ years, the Bakun Index has served as an instrumental resource in oceanographic and fisheries research along the eastern Pacific margin, employed in wide-ranging studies covering, for example, physics (Enfield & Allen, 1980), phytoplankton (Small & Menzies, 1981), zooplankton (Brodeur & Ware, 1992), fish (Parrish et al., 1981), elephant seals (Reiter et al., 1978), and whales (Croll et al., 2005).

In this paper we introduce new upwelling indices for the U.S. West Coast, and to motivate the development of these indices we revisit existing indices and their underlying principles. In section 2, we briefly review the most relevant points of Ekman theory. In section 3, we discuss the Bakun Index, including its methodology, assumptions, and shortcomings. In section 4 we present upwelling indices that leverage technological and scientific advances realized since the introduction of the Bakun Index, and in the following sections we compare the different indices and discuss nuances of their application.

2. Revisiting Ekman Theory

For the purposes of this discussion, it is convenient to apply a locally valid Cartesian coordinate system with x, y, and z aligned eastward, northward, and upward, respectively, and with their corresponding velocities denoted by u, v, and w. Ekman theory assumes a linear, homogenous ocean in steady state, with no lateral gradients and a laterally infinite domain. Under these conditions, the equations of motion reduce to a balance between the Coriolis and frictional forces,

$$fv = -\frac{1}{\rho_0}\frac{\partial \tau^x}{\partial z} \quad fu = \frac{1}{\rho_0}\frac{\partial \tau^y}{\partial z} \tag{1}$$

where f is the Coriolis parameter, ρ_0 is a reference density for seawater, and viscous stresses in the eastward and northward directions are represented by τ^x and τ^y, respectively. Integrating equation (1) from a depth where internal stresses vanish (usually referred to as the *Ekman depth*) to the surface gives relationships for northward and eastward volume transports per unit length (V^{Ek} and U^{Ek}; units of m^2/s) as a function of eastward and northward surface wind stress ($\tau_0{}^x$ and $\tau_0{}^y$), respectively:

$$V^{Ek} = \frac{-\tau_0^x}{\rho_0 f} \quad U^{Ek} = \frac{\tau_0^y}{\rho_0 f} \tag{2}$$

Equation (2) predicts integrated near-surface transport directed 90° to the right (left) of the surface wind stress in the northern (southern) hemisphere. Ekman also derived an expression for the vertical structure of the horizontal motion, assuming a constant vertical viscosity and internal stresses proportional to vertical shear in horizontal velocity. The celebrated solution to this problem has surface currents directed 45° to the right (left) of the surface wind stress in the northern (southern) hemisphere, with horizontal velocities weakening and rotating with depth to the right (left) to form a spiral. Though the theoretical solution for horizontal currents depends on the structure of vertical viscosity, which in nature relates to turbulent processes and varies in time and space, the Ekman spiral has been observed in time-averaged flows (Chereskin, 1995). In

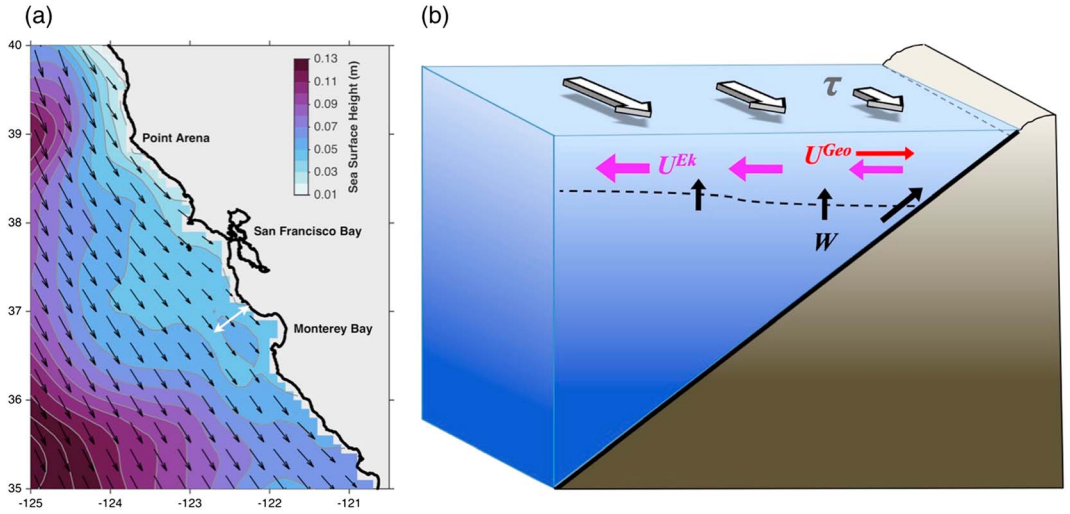

Figure 1. (a) Mean 1988–2017 sea surface height (in color) and wind stress (arrows) during the upwelling season (March–August) off the central/northern California coast, obtained from the California Current System Regional Ocean Modeling System reanalyses; (b) schematic representation of a coastal section corresponding to the white line in (a), showing key components of the upwelling dynamics of central importance to this paper: Alongshore wind stress (τ), an alongshore sea surface height gradient, Ekman transport ($\boldsymbol{U^{Ek}}$), geostrophic transport ($\boldsymbol{U^{Geo}}$), vertical transport (W), and the depth of the surface mixed layer (dashed line).

contrast, as equation (2) shows, the vertically integrated Ekman transport, which is the critical quantity of interest for upwelling, is fortuitously independent of the magnitude and structure of the vertical viscosity.

Near oceanic eastern boundaries, which typically have nominally meridional orientation, equatorward wind stress drives westward (i.e., offshore) Ekman transport (Figure 1). Since the velocity across the coastal boundary is zero, offshore Ekman transport results in cross-shelf mass flux divergence (hereafter referred to as *coastal divergence*) that must be compensated by mass flux convergence in the alongshore or vertical directions. Assuming no alongshore variations, water displaced offshore must be compensated from below, and the wind-driven Ekman transport is equal to the vertical transport into the Ekman layer. This description forms the basis of the Bakun Index, discussed in the following section.

In addition to upwelling that results from coastal divergence, vertical transport can be driven also by Ekman transport divergence associated with spatial variability in wind stress, specifically wind stress curl (Figure 1). The wind stress curl-driven vertical velocity at the base of the Ekman layer, w_e, is given by

$$w_e = \frac{1}{\rho f}\left(\frac{\partial \tau_0^y}{\partial x} - \frac{\partial \tau_0^x}{\partial y}\right) \tag{3}$$

where w_e is the vertical velocity at the base of the Ekman layer. In the northern hemisphere, positive curl drives Ekman transport divergence and draws water from depth into the Ekman layer (positive w_e; upwelling), a process referred to as *Ekman suction*. Negative curl drives negative w_e, called *Ekman pumping*, as Ekman transport convergence pumps near surface water downward into the ocean interior. In the southern hemisphere, where f is negative, positive and negative wind stress curl are associated with Ekman pumping and Ekman suction, respectively. While wind stress structure results in Ekman pumping over most of the ocean basin at subtropical latitudes, curl-driven upwelling is ubiquitous near eastern boundaries, where land and coastal orography increase drag on near-surface winds and result in a decrease in wind stress magnitude near the coast relative to that offshore (Renault, Hall, & McWilliams, 2016). This decline in wind stress amplitude produces wind stress curl that is positive (upwelling favorable) in the case of equatorward winds and negative (downwelling favorable) in the case of poleward winds. Past efforts have sought to distinguish upwelling due to coastal divergence from upwelling due to wind stress curl, in terms of both their magnitude (e.g., Pickett & Paduan, 2003) and their ecological impacts (e.g., Rykaczewski & Checkley, 2008). However, they are not spatially distinct. Even in the absence of wind stress curl, subsurface isopycnals tilt over cross-shore scales of tens of kilometers at midlatitude, and upwelling can extend even farther offshore over wide

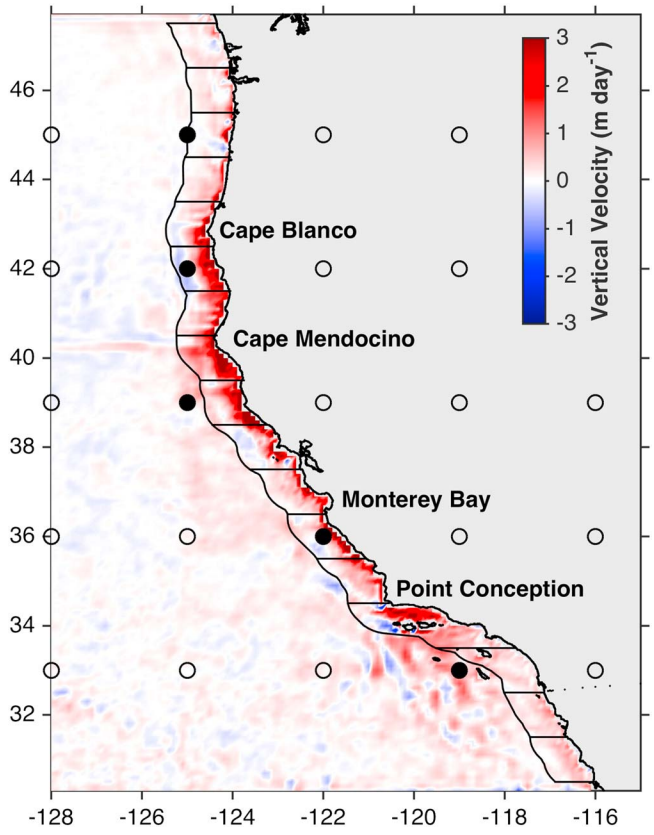

Figure 2. Mean 1988–2017 vertical velocity at the base of the mixed layer during the upwelling season (March–August), obtained from the Regional Ocean Modeling System reanalyses. The 3° Fleet Numerical Meteorology and Oceanography Center sea level pressure grid is overlaid, with filled circles indicating locations used historically for calculation of the Bakun Index. Black lines outline regions of integration for the new upwelling indices.

shelves, with sustained upwelling favorable winds, and in regions of strong stratification (Barton et al., 1977; Estrade et al., 2008; Jacox & Edwards, 2011; Lentz & Chapman, 2004). Similarly, curl-driven upwelling can be important very close to shore, particularly in the lee of capes and headlands where expansion fans in the marine boundary later occur within tens of kilometers of the coast (Dever et al., 2006; Fiechter et al., 2014; Koračin & Dorman, 2001; Pickett & Paduan, 2003). Furthermore, wind products with higher spatial resolution show the coastal wind drop-off occurring in a narrower coastal band (Capet et al., 2004), increasing the overlap of estimated upwelling due to coastal divergence and wind stress curl. Thus, while upwelling variability near shore is out of phase with upwelling variability farther offshore (Jacox et al., 2014), neither can be attributed solely to coastal divergence or wind stress curl.

3. Revisiting the Bakun Index

The Bakun Index methodology was originally laid out in two technical reports (Bakun, 1973, 1975) that while highly cited are challenging to obtain. A more accessible report by Schwing et al. (1996) also details the Bakun Index calculation, and we review it here. While some of the details of the Bakun Index calculation have changed over time, the methodology has not. Here we present the original calculation described by Bakun (1973) and implemented by NOAA. After this overview we describe changes employed in subsequent iterations of the index.

An estimate of sea level pressure (SLP) is obtained from an operational atmospheric model run by the U.S. Navy's Fleet Numerical Meteorology and Oceanography Center (FNMOC), formerly the Fleet Numerical Weather Center. SLP gradients are then estimated at the grid points corresponding to upwelling index locations (Figure 2) by calculating the pressure difference between grid points on either side and dividing by the distance between them. Because the initial FNMOC grid resolution was 3°, the pressure gradients ($\partial SLP/\partial y$ and $\partial SLP/\partial x$) are calculated across 6° of latitude and longitude, respectively. Geostrophic wind speeds are obtained from the pressure gradients according to

$$u_g = -\frac{1}{\rho_a f}\frac{\partial SLP}{\partial y} \quad v_g = \frac{1}{\rho_a f}\frac{\partial SLP}{\partial x} \tag{4}$$

where ρ_a represents air density, assumed constant at 0.00122 g/cm^2. Surface wind speed is estimated by rotating the geostrophic wind 15° counterclockwise and reducing its magnitude by 30% to approximate effects of friction at the sea surface. The surface wind stress vector $\boldsymbol{\tau}$ is computed from the wind speed vector $\boldsymbol{v}$ using a bulk formulation

$$\boldsymbol{\tau} = \rho_a c_d |\boldsymbol{v}| \boldsymbol{v} \tag{5}$$

where c_d is a nondimensional drag coefficient, assumed to be 0.0026 for the monthly mean pressure data used in Bakun (1973). Finally, the alongshore component of $\boldsymbol{\tau}$, estimated using the mean coastline angle over ~200 miles, is used in equation (2) to compute offshore Ekman transport (i.e., the Bakun Index).

Three versions of the Bakun Index are available from NOAA (see acknowledgments for data sources), and they differ in two ways: the characteristics of SLP fields used as input and the calculation of wind stress from wind speed. The original index (Bakun, 1973), which extends back to 1946, was calculated using monthly averaged SLP on a 3° grid, and a relatively high drag coefficient of 0.0026 was used in equation (5) to account for the monthly averaging of SLP. Bakun (1975) presented a second version of the index using 6-hourly SLP fields and a lower drag coefficient (0.0013); this version extends back to 1967. In 1996, FNMOC began

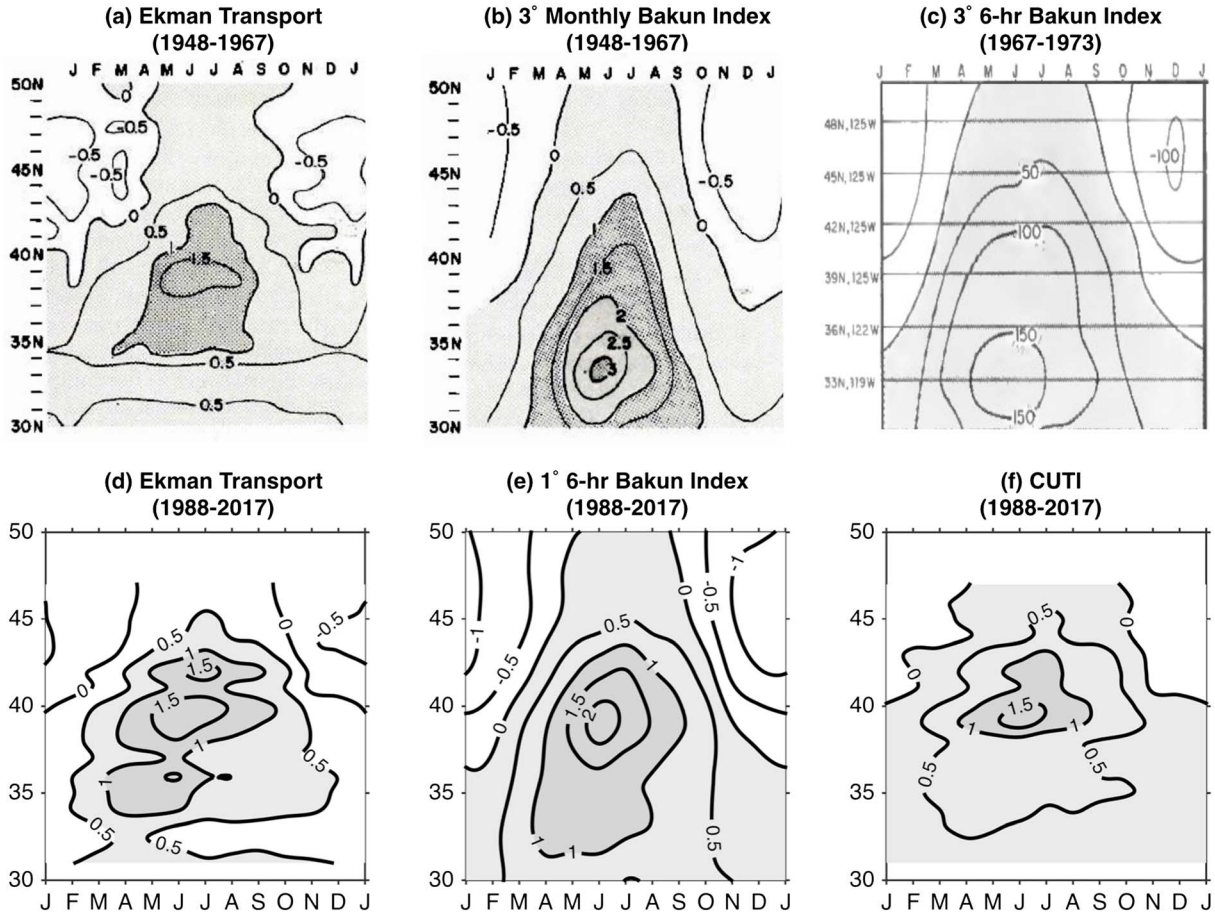

Figure 3. Climatological transport estimates are plotted against latitude for (top) transport indices as described by Bakun (1973, 1975): (a) Ekman transport estimated from in situ wind measurements (adapted from Bakun, 1973), (b) Bakun Index calculated from monthly 3° sea level pressure (SLP) fields (adapted from Bakun, 1973), (c) Bakun Index calculated from 6-hourly 3° SLP fields (adapted from Bakun, 1975) and (bottom) transport indices calculated 1988–2017: (d) Ekman transport estimated from California Current System Regional Ocean Modeling System reanalysis winds, (e) Bakun Index calculated from 6-hourly 1° SLP fields, (f) revised upwelling index (Coastal Upwelling Transport Index) described herein. Note that panel (c) uses units of m^3/s per 100-m coastline, so values are a factor of 100 greater than in the other panels, which use units of m^3/s per meter coastline (i.e., m^2/s).

providing SLP on a 1° global grid. For consistency, the historical upwelling indices continued to be calculated from 3° pressure fields, which were interpolated from the 1° grid (Schwing et al., 1996). The third, and most recent, version of the index uses the 1° pressure fields for 1996 to present and the native FNMOC resolution prior (~3° for 1967–1980 and ~2.5° for 1981–1996). This version also replaces the constant drag coefficients of the previous two with a wind speed-dependent parameterization based on Large and Pond (1981) modified for low wind speeds as in Trenberth et al. (1990). In the remaining text and associated figures, we refer to these three versions of the Bakun Index as 3° monthly, 3° 6 hr, and 1° 6 hr, respectively.

Differences between computations of each Bakun Index version are consequential—they impact both the spatial patterns and magnitudes of upwelling estimates (Figure 3). In the seasonal cycle, the change from monthly to 6-hr winds greatly reduced the magnitude of the upwelling index in the southern California Current system (CCS), but both of these products computed from 3° pressure fields have a spatial structure where the latitude of maximum upwelling is much farther south than that computed from wind observations (~33°N vs. ~39°N; cf. Figures 3a–3c). This issue was noted at the outset by Bakun (1975) who wrote that "a spatial distortion in absolute magnitude results in noncomparability of numerical values between different locations" and advised that "because of uncertainties in some of the constants employed and for other reasons outlined in this report, it may be well to consider these indices as indicative of relative fluctuations rather than as quantitative measures of absolute magnitude." Furthermore, FNMOC has periodically changed the details of its SLP field generation and indices prior to 1962 were constructed using SLP fields from sources

other than FNMOC. These inconsistencies in SLP induce changes in the Bakun Index through time and must be considered when analyzing long-term trends and variability in upwelling (Schwing et al., 1996).

In addition to uncertainties in the Ekman transport calculation, the Bakun Index does not (and does not try to) capture several important contributors to upwelling dynamics. First is wind stress curl-driven upwelling associated with alongshore wind gradients (i.e., $d\tau_0^x/dy$ for a coastline oriented in the y-direction), though the Bakun Index does inherently include wind stress curl-driven upwelling associated with zonal gradients in the alongshore wind stress (i.e., $d\tau_0^y/dx$) inshore of the location where the index is calculated. Second is the contribution of the cross-shore geostrophic flow. If the constraint of no horizontal pressure gradient is removed from Ekman theory, equation (1) for the zonal velocity becomes

$$fu = \frac{1}{\rho}\frac{\partial \tau^y}{\partial z} - g\frac{\partial \eta}{\partial y} \tag{6}$$

and equation (2) becomes

$$U^{Ek} + U^{geo} = \frac{\tau_0^y}{\rho f} - \frac{gD}{f}\frac{\partial \eta}{\partial y} \tag{7}$$

where η is the free surface height, g is the gravitational acceleration, and U^{geo} is the zonal geostrophic transport. The Ekman layer depth is given by D, which itself depends on the magnitude and structure of the turbulent viscosity. In subtropical EBUS regions, D generally extends meters to tens of meters. Equation (6) argues that the near surface cross-shore transport is the sum of the Ekman transport and the cross-shore geostrophic transport associated with an alongshore pressure gradient (Figure 1). Cross-shore geostrophic transport can substantially alter the vertical transport relative to wind-based estimates (Colas et al., 2008; Jacox et al., 2014; Marchesiello & Estrade, 2010; Rossi et al., 2013), and including the geostrophic component is also important to understand how future changes in wind (e.g., Rykaczewski et al., 2015) will translate to changes in upwelling (e.g., Oerder et al., 2015). Third, Ekman theory does not consider the properties of upwelled water. Upwelling drives productivity by delivering nutrients to the euphotic zone, but the Bakun Index does not capture changes in the quality of upwelled waters. For example, in simple two-dimensional models, stratification modifies the vertical structure of upwelling, particularly the source depth of upwelled waters and consequently their nutrient content (e.g., Jacox & Edwards, 2011, Lentz & Chapman, 2004), but it does not modify the volume transport (see equations (2) and (3)) and therefore is not reflected in the Bakun Index.

4. Improved Upwelling Indices for the U.S. West Coast

We introduce two new upwelling indices aimed at addressing the shortcomings outlined above, primarily by leveraging technological advances realized since the introduction of the Bakun Index. First is the Coastal Upwelling Transport Index (CUTI, pronounced "cutie"), which is comparable to the Bakun Index in that it is an estimate of the total volume of water upwelled or downwelled in a given time period (i.e., the vertical volume flux into or out of the surface layer). Second is the Biologically Effective Upwelling Transport Index (BEUTI, pronounced "beauty"), which is an estimate of the total quantity of nitrate upwelled or downwelled in a given time period (i.e., the vertical nitrate flux into or out of the surface layer). BEUTI therefore quantifies not only the intensity of upwelling but also the quality of upwelled waters in terms of their nutrient content, which can strongly influence productivity independent of the surface wind strength (Jacox, Bograd, et al., 2015; Jacox et al., 2016). Both indices rely on ocean and atmosphere state estimates obtained from a data-assimilative regional ocean model configured for the CCS. The spatial coverage of CUTI and BEUTI is from 31 to 47°N along the North American West Coast, and the temporal coverage is from 1988 to present. In the following sections, we provide details of the ocean model and the calculation of the new upwelling indices.

4.1. CCS ROMS Reanalyses

Ocean state estimates and surface wind forcing are obtained from historical reanalyses of the CCS produced using the Regional Ocean Modeling System (ROMS) with 4-dimensional variational data assimilation. Several reanalysis products are available: the first spans 31 years (1980–2010) and is hereafter referred to as CCSRA31, the second spans 14 years (1999–2012; CCSRA14), and the last covers 2011 to present and is updated in near real time (CCSNRT). All three reanalyses share a common grid, which spans approximately the U.S. West Coast

(30–48°N) and extends offshore to 134°W with 0.1° horizontal resolution and 42 terrain-following vertical levels. CCSRA31 and CCSRA14 are described in detail by Neveu et al. (2016) and differ only in their surface forcing; CCSRA31 uses a combination of the European Center for Medium-Range Weather Forecasts ERA-40 and ERA-Interim reanalyses and Cross-Calibrated Multi-Platform winds, while CCSRA14 uses higher-resolution output from the Naval Research Laboratory Coupled Ocean/Atmosphere Mesoscale Prediction System. Both CCSRA31 and CCSRA14 are forced at the lateral boundaries by output from the Simple Ocean Data Assimilation ocean reanalysis. CCSNRT (http://oceanmodeling.ucsc.edu/ccsnrt/; Moore et al., 2013) also uses the Coupled Ocean/Atmosphere Mesoscale Prediction System for surface boundary conditions but is forced at the lateral boundaries by the Naval Research Laboratory's 1/12° global HYCOM nowcast. In all cases, surface fluxes are calculated within ROMS using the bulk formulations of Liu et al. (1979); Fairall, Bradley, Godfrey, et al. (1996); and Fairall, Bradley, Rogers, et al. (1996). Therefore, we use surface wind stresses from the ROMS output in our upwelling indices, though in theory one could use the atmospheric models directly for Ekman transport calculation. All three ocean reanalyses assimilate sea surface temperature and sea surface height (SSH) data from satellites as well as available in situ temperature and salinity measurements obtained from ships and autonomous platforms. All ROMS variables are daily averaged for upwelling index calculation.

It should be noted that the new upwelling indices described below rely on merging multiple ocean reanalyses (CCSRA31, CCSRA14, and CCSNRT) to cover the full period described. To account for the change to a higher-resolution forcing from CCSRA31 to CCSRA14, we adjusted the CCSRA31-derived indices to match the mean and standard deviation of the CCSRA14-derived indices during a 10-year period of overlap (2001–2010; supporting information Figures S1 and S2). CCSRA14 and CCSNRT also differ in that the surface forcing can be adjusted during data assimilation in CCSRA14 but not in CCSNRT. We find any influence of this change on Ekman transport estimates to be negligible. At present, we provide CUTI and BEUTI beginning in 1988, the earliest availability of the relatively high-resolution (0.25°) Cross-Calibrated Multi-Platform wind product. In the future we plan to use a single self-consistent regional ocean reanalysis to generate the upwelling indices, and we will likely be able to extend the upwelling indices further back in time.

4.2. CUTI

CUTI is designed to provide estimates of the rate of vertical volume transport at multiple locations along the U.S. West Coast. It is similar in that regard to the Bakun Index and has the same units (volume of vertical transport per second per meter of coastline). However, CUTI incorporates improved estimates of the Ekman transport and accounts for cross-shore geostrophic flow associated with an alongshore SSH gradient. CUTI is calculated for bins spanning 1° of latitude and extending 75 km offshore to capture the band of wind-driven upwelling associated with elevated nitrate concentrations and phytoplankton biomass (Figure 2; Jacox et al., 2016).

4.2.1. Calculating CUTI

We define CUTI as the sum of Ekman transport ($\boldsymbol{U^{Ek}}$) and cross-shore geostrophic transport ($\boldsymbol{U^{geo}}$), as in equation (6), an approach that has been applied previously to coastal upwelling systems (Marchesiello & Estrade, 2010; Rossi et al., 2013). Upwelling indices here are derived from ocean reanalysis output, with the Ekman and geostrophic contributions to vertical transport calculated as follows.

Ekman volume transports in the meridional and zonal directions are calculated from the surface wind stress and the Coriolis frequency (equation (2)). Zonal and meridional Ekman transports are integrated around the perimeter of each 1° latitudinal bin (Figure 2) to obtain a total Ekman transport into/out of the region. This method accounts for Ekman transport associated with alongshore wind stress as well as wind stress curl in both the alongshore and cross-shore directions. In contrast, Ekman transport estimated from alongshore wind stress at some offshore location (as in the Bakun Index) omits Ekman suction/pumping associated with alongshore wind stress gradients.

Cross-shore geostrophic velocity ($\boldsymbol{u^{geo}}$) is estimated from the alongshore SSH gradient according to

$$\boldsymbol{u^{geo}} = \frac{g}{f}\frac{\Delta SSH}{d_{coast}} \tag{8}$$

where ΔSSH is the difference between coastal SSH values at the northernmost and southernmost grid points in each 1° bin, and d_{coast} is the distance (m) between those same points. For each grid point, each day, mixed

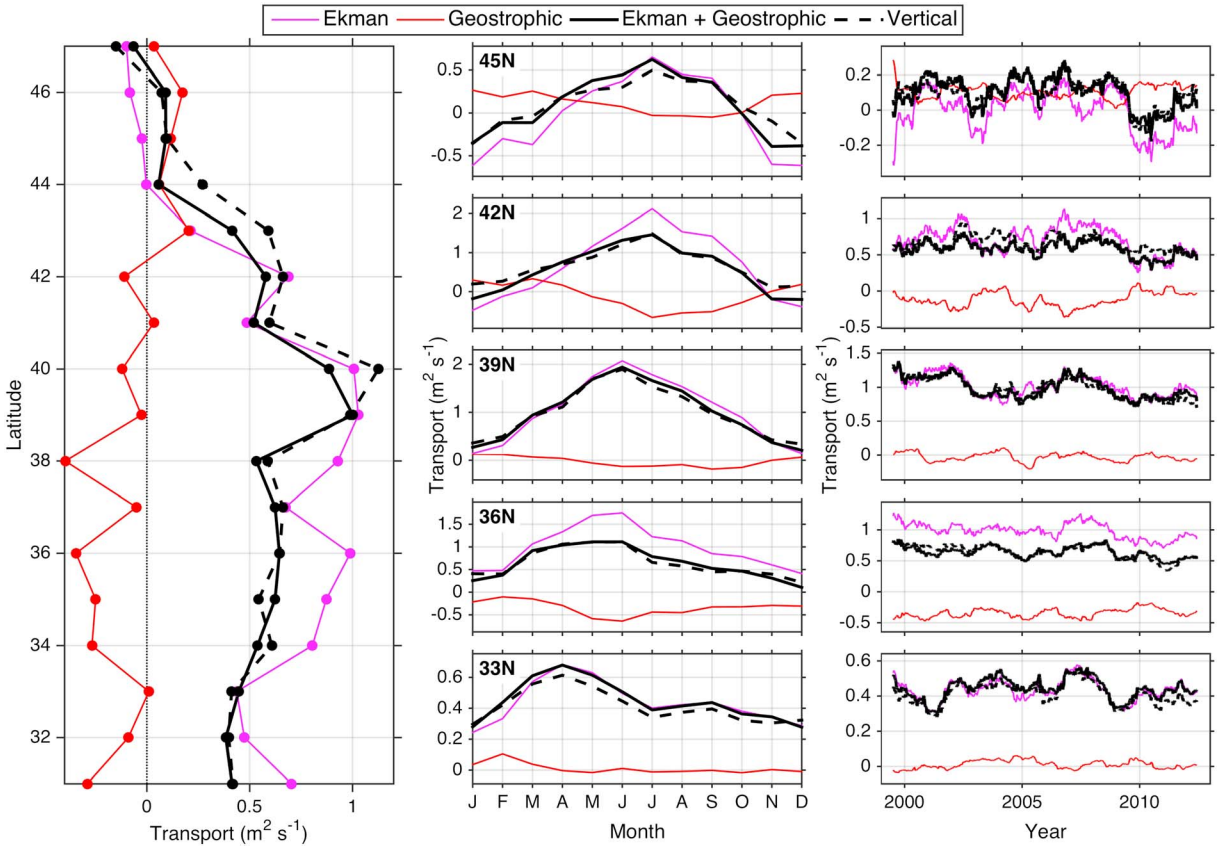

Figure 4. (left) Long-term mean, (middle) seasonal climatology, and (right) interannual variability of transport components, plotted against latitude (left panel) or at select latitudes (middle and right panels). Positive values are upwelling favorable. Transport components were calculated from CCSRA14 for 1999–2012 (see sections 4.1 and 4.2). Interannual variability was calculated by smoothing daily time series with a 12-month running mean. The temporal coverage of the new indices is longer (1988 to present), but they are constructed from multiple reanalyses. Here we focus on a single self-consistent reanalysis to explore individual terms in the transport budget. Note scale differences on *y*-axes of middle and right panels.

layer depth (MLD) is calculated according to Kara et al. (2000) using the density change associated with a 0.8 °C temperature change. In cases where the mixed layer extends to the seafloor, MLD is equal to the bottom depth. For the geostrophic transport calculation, MLD is averaged within 30 km of the coast (approximately the Rossby radius of deformation) for each 1° latitude bin, and cross-shore geostrophic transport is estimated assuming geostrophic velocity is constant throughout the MLD ($\boldsymbol{U^{geo}} = \boldsymbol{u^{geo}} * MLD$).

One may question why we use the combination of Ekman and geostrophic transports to calculate CUTI, rather than extracting vertical velocities directly from the ocean model. We show that modeled vertical velocities are approximated well by the sum of Ekman and cross-shore geostrophic transports (section 4.3 and Figures 4 and 5). However, we do not use modeled vertical velocities to construct the index for several reasons: First, the calculation of upwelling using modeled vertical velocity is not straightforward. One must first define a representative depth at which vertical velocity is extracted (e.g., the MLD), which will be different for each grid cell, making it difficult to close the transport budget. For example, when the MLD differs between adjacent grid cells, water can enter/exit the surface mixed layer horizontally and that component of the transport will be missed from the upwelling/downwelling estimate. Second, an index constructed from Ekman and geostrophic transports is much more amenable to application outside of the CCS, particularly where high-resolution ocean reanalyses are unavailable. In principle, CUTI can be derived for any region with reasonable data sets for surface wind stress and alongshore SSH gradients, and similar indices have been presented elsewhere (e.g., Rossi et al., 2013). However, recreating CUTI from surface (e.g., remote sensing) observations alone introduces additional assumptions and uncertainties, which are discussed further in section 7.

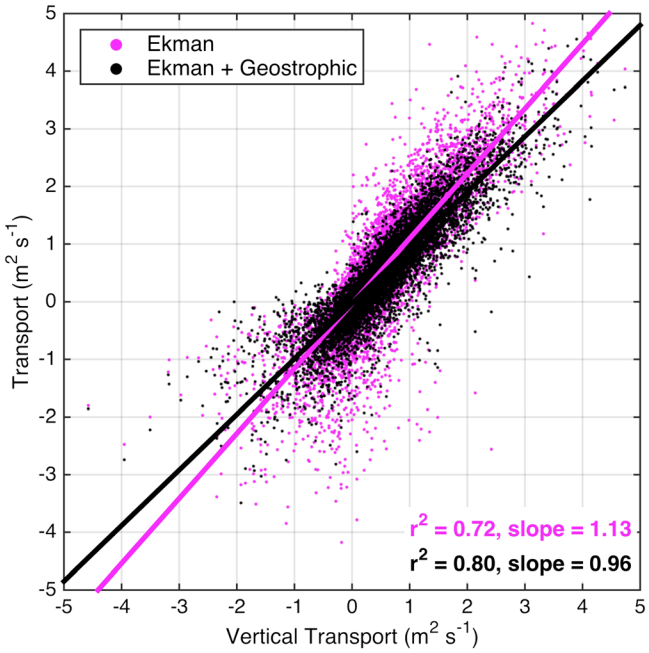

Figure 5. Ekman transport (purple) and Ekman + geostrophic transport (i.e., Coastal Upwelling Transport Index; black) are plotted versus modeled vertical transport. Solid lines indicate linear regressions to the data; variance explained and slopes of regression lines are shown at bottom right. Transport values are weekly averages computed from CCSRA14 for 1999–2012.

4.2.2. Contribution of Ekman Transport to CUTI

Variability in the wind-driven transport off the U.S. West Coast has been explored extensively over decades of research, so we describe it only briefly here. In the mean, Ekman transport in recent decades is offshore (upwelling-favorable) south of ~44°N and onshore (downwelling favorable) farther north (Figure 4). At all latitudes a seasonal cycle of Ekman transport is evident, and the climatological date of peak offshore transport occurs earlier in the south (April at 33°N) than in the north (July at 45°N). Spring/summer Ekman transport is strongest from 36 to 42°N, and the northern CCS experiences strong onshore Ekman transport in the wintertime while in the central and southern CCS Ekman transport is offshore year-round (Figure 4). Finally, there is considerable interannual variability in Ekman transport, with enhanced equatorward winds (and therefore offshore Ekman transport) associated with negative phases of the El Niño-Southern Oscillation and Pacific Decadal Oscillation, and positive phases of the North Pacific Gyre Oscillation and the Northern Oscillation Index (Chhak & Di Lorenzo, 2007; Di Lorenzo et al., 2008; Jacox et al., 2014; Jacox, Fiechter et al., 2015; Schwing et al., 2002).

4.2.3. Contribution of Geostrophic Transport to CUTI

Model output indicates a negative correlation between cross-shore geostrophic transport and Ekman transport, in both space and time (Figure 4). Mean geostrophic transport is most strongly onshore at latitudes of 34–38°N, where offshore Ekman transport is also strong. However, mean cross-shore geostrophic transport from 39 to 41°N is near zero despite Ekman transport that is on average strongly offshore (Figure 4), a result of flows that separate from coastal promontories (Point Arena, Cape Mendocino) and provide an offshore contribution to the geostrophic transport (Marchesiello & Estrade, 2010). North of 42°N, mean offshore geostrophic transport is associated with onshore Ekman transport. Seasonal cycles of Ekman transport and geostrophic transport are also negatively correlated, with onshore geostrophic flow most prominent in the spring/summer and, like Ekman transport, peaking later in the year at more northern latitudes (Figure 4). Connolly et al. (2014) found similar latitudinal and seasonal variability in the alongshore structure of SSH from tide gauge observations, a numerical ocean model, and a coastal trapped wave model. In particular they found a negative SSH gradient (onshore geostrophic flow) along the U.S. West Coast during summer and a positive SSH gradient (offshore geostrophic flow) north of 40°N in winter.

4.2.4. Evaluation of CUTI Relative to Individual Transport Components

The sum of geostrophic and Ekman transport agrees quantitatively with modeled vertical transport in the long-term mean, monthly climatology, and interannual variability (Figure 4) as well on shorter timescales (e.g., weekly; Figure 5). This agreement, in spite of uncertainties in vertical transport calculations described earlier, implies that to first order the alongshore momentum balance is between the wind stress, alongshore pressure gradient, and Coriolis force, consistent with a number of previous studies of eastern boundary current systems (Allen & Smith, 1981; Brown et al., 1987; Hickey, 1984; Lentz, 1994; Lentz & Chapman, 2004). On event timescales (~1 week), Ekman transport alone captures 72% of the variance in modeled vertical transport, and the two are linearly related with a regression slope of 1.13, indicating that Ekman transport overestimates vertical transport. The inclusion of geostrophic transport in CUTI improves agreement with vertical transport, capturing 80% of the variance with a regression slope of 0.96 (Figure 5). Thus, the geostrophic contribution reduces upwelling estimates on average by ~15% relative to Ekman transport, though that relationship is latitude dependent. Notably, while Ekman transport overestimates vertical transport, the regression line between the two still crosses through (0,0), indicating that cross-shore geostrophic transport tends to oppose Ekman transport whether it is upwelling or downwelling favorable (Figure 5) and supporting the notion that at least on short (weekly) timescales, the alongshore surface pressure gradient sets up in response to the local wind. On longer timescales, the surface pressure gradient is influenced more strongly by remote (greater than O[100 km] away) wind variability and subsequent coastal trapped wave propagation (e.g., Verdy et al., 2014).

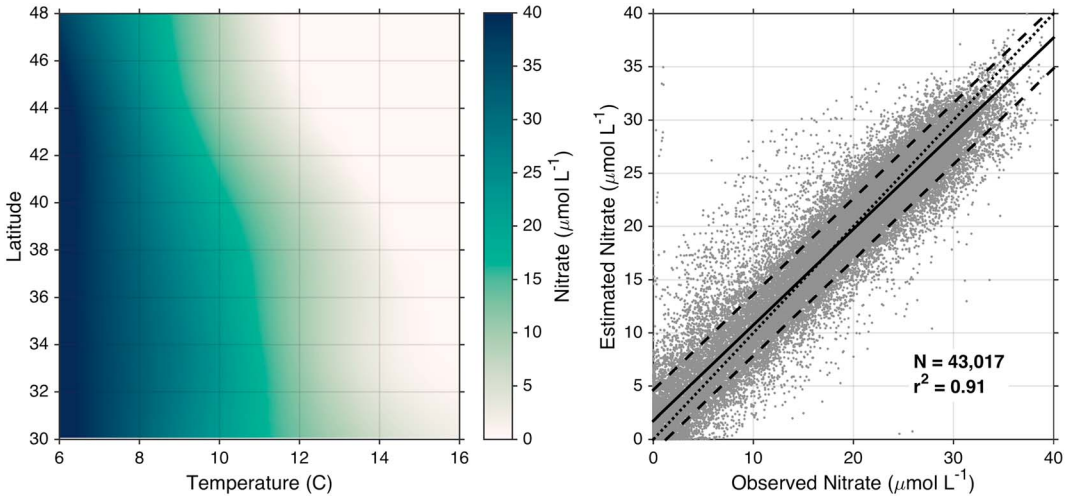

Figure 6. (left) Nitrate fitted as a function of temperature and latitude in the California Current System. (right) Nitrate estimated from the temperature-latitude-nitrate relationship plotted against observed nitrate, with total number of data points (N) and fraction of variance explained (r^2). Black lines are a linear regression through the data (solid), ±1 standard deviation (dashed), and the 1:1 line (dotted). Data were obtained from the World Ocean Database, CalCOFI, GLOBEC, and the NCEI database and were constrained to post-1987, from 30 to 48°N, within 75 km of shore, and from 20 to 200 m depth.

4.3. BEUTI

BEUTI is an estimate of nitrate flux into the surface mixed layer and is intended to move beyond physical upwelling transport indices (e.g., the Bakun Index or CUTI) to provide an index that better captures bottom-up drivers of productivity in the CCS. The vertical nitrate flux (i.e., BEUTI) is calculated as the product of the estimated vertical transport (i.e., CUTI) and nitrate concentration at the base of the mixed layer (Jacox, Bograd, et al., 2015). The methodology outlined for CUTI in section 4.2 therefore applies here as well and is supplemented by an estimate of the nitrate content in upwelled waters. Nitrate concentration at the base of the mixed layer is estimated from the physical ocean reanalysis output by (i) estimating MLD from temperature and salinity profiles according to Kara et al. (2000); (ii) extracting temperature at the base of the mixed layer, and (iii) using temperature and latitude to estimate nitrate concentration from an empirically derived temperature-latitude-nitrate relationship that captures >90% of observed variance in ~43,000 historical observations obtained from multiple observational programs along the U.S. West Coast (Figure 6).

Subsurface nitrate concentration, like upwelling, varies considerably on multiple spatial and temporal scales (Figure 7). In the time mean, nitrate concentration at the base of the mixed layer is closely related to MLD; a relatively shallow mixed layer in the Southern California Bight coincides with low nitrate concentrations, while the deepest mean MLDs and highest mean nitrate concentrations occur off northern California (38–40°N). The climatological seasonal cycle of MLD exhibits deepest values in winter while peak nitrate concentrations occur in spring at most latitudes, concurrent with the onset of seasonal upwelling. Indeed, upwelling and subsurface nitrate concentration are positively correlated in space and time as strong upwelling draws nitrate-rich water toward the surface (Jacox et al., 2016). However, there are times when the two are decoupled. For example, in the northern CCS in winter, vertical transport tends to be weakly upwelling or downwelling but subsurface nitrate concentrations are high due to deep mixing (Figure 7). It is in cases where upwelling and subsurface nitrate concentrations are decoupled that an index capturing nitrate variability is particularly useful, and such cases are discussed in more detail in section 6 as well as in Jacox et al. (2016).

5. Comparing Bakun Indices and CUTI

Having described the development of new upwelling indices for the U.S. West Coast, we turn to the question of how various available indices differ from each other. First, we compare the three versions of the Bakun Index, keeping in mind that differences between these indices arise solely from changes in the spatial and temporal resolution of SLP data, and in the assumptions employed to estimate wind stress from wind speed. In some cases, the difference between two versions of the Bakun Index is even greater than the difference between the most recent Bakun Index and CUTI (Figure 8). In particular, changing from monthly to hourly

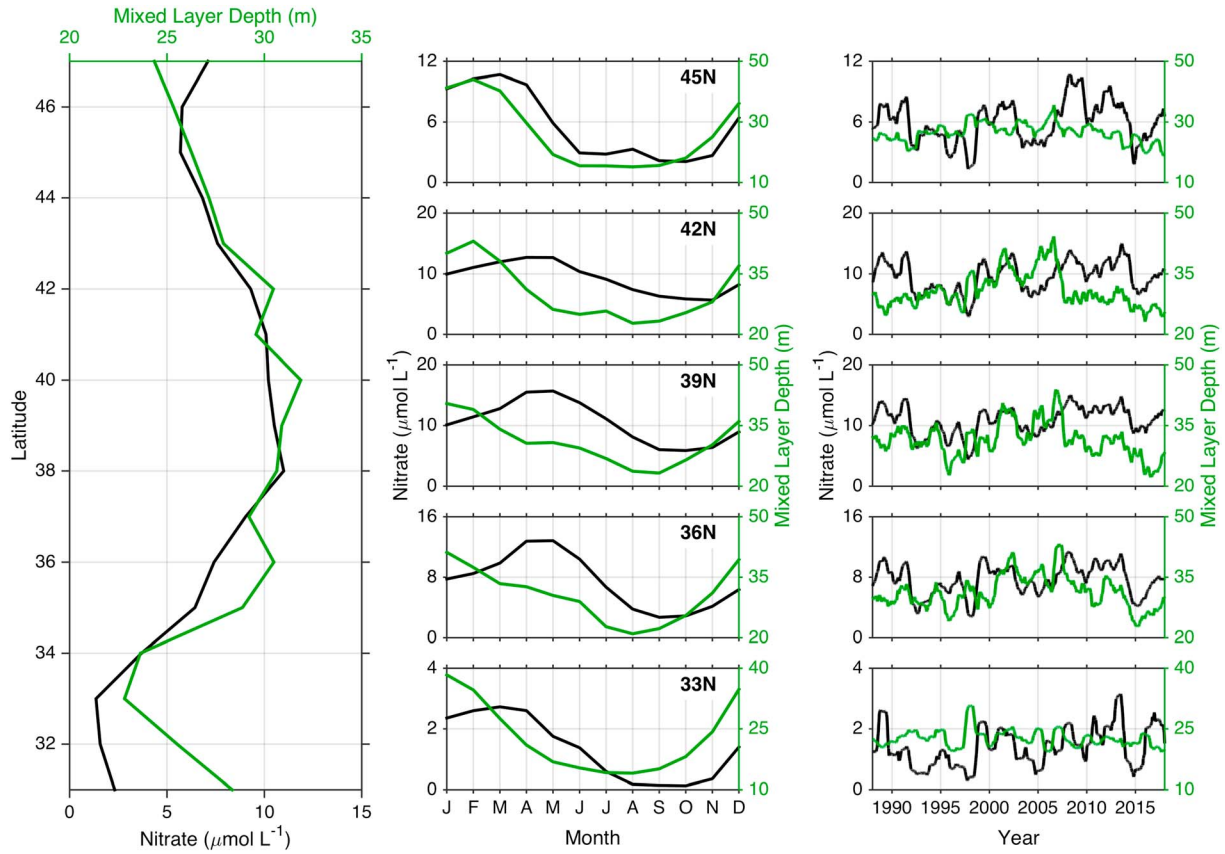

Figure 7. (left) Long-term mean, (middle) seasonal climatology, and (right) interannual variability of nitrate concentration at the base of the mixed layer (black) and mixed layer depth (green), plotted against latitude (left panel) or at select latitudes (middle and right panels). Nitrate concentrations were estimated using temperature from the West Coast Regional Ocean Modeling System reanalyses and latitude as input to the latitude-temperature-nitrate fit in Figure 5. These subsurface nitrate values are multiplied by the Coastal Upwelling Transport Index to produce the Biologically Effective Upwelling Transport Index. Note scale differences on *y*-axes of middle and right panels.

data dramatically reduced the estimated upwelling strength off the central and southern California coast, and changing from 3° to 1° data improved the latitudinal gradient in seasonal upwelling climatology (Figures 4 and 8). Therefore, even when using a Bakun Index, one must be aware of the version being used and its strengths and limitations. The 3° monthly index provides long (~70 years to date) and relatively consistent time series but carries the greatest uncertainty due to low spatial and temporal SLP resolution. The 3° 6-hr index more accurately captures temporal wind variability and is a better option provided the slightly shorter duration (~50 years) is adequate. The 1° 6-hr index is best of the three for the post-1996 period when FNMOC has provided SLP fields at 1° resolution, but due to changes in the native SLP resolution prior to 1996 it is perhaps the least consistent product for use over its entire duration (1967 to present). Differences between Bakun indices are most pronounced south of 39°N, while farther north they are largely in agreement with each other and with CUTI (Figures 8 and 9).

Differences between CUTI and Bakun Indices can be attributed to multiple sources; some arise in the estimation of Ekman transport (e.g., wind field estimation, wind stress calculation from wind speed, handling of wind stress curl, and where indices are computed; cf. blue and purple lines in Figure 8), and further differences arise from CUTI's inclusion of information on the ocean state (i.e., the SSH field; cf. purple and black lines in Figure 8). Relative to CUTI, Bakun Indices tend to overestimate upwelling south of 39°N and overestimate downwelling north of 39°N (Figures 8 and 9). These differences vary seasonally with largest difference at the locations and times of strongest vertical transport, particularly during the spring/summer upwelling season in the southern half of the domain and the winter downwelling season in the northern half of the domain. As discussed in section 4.2, these biases are qualitatively consistent with the effects of including/omitting cross-shore geostrophic transport from upwelling estimates. At 33°N, upwelling that occurs farther offshore than the 75 km

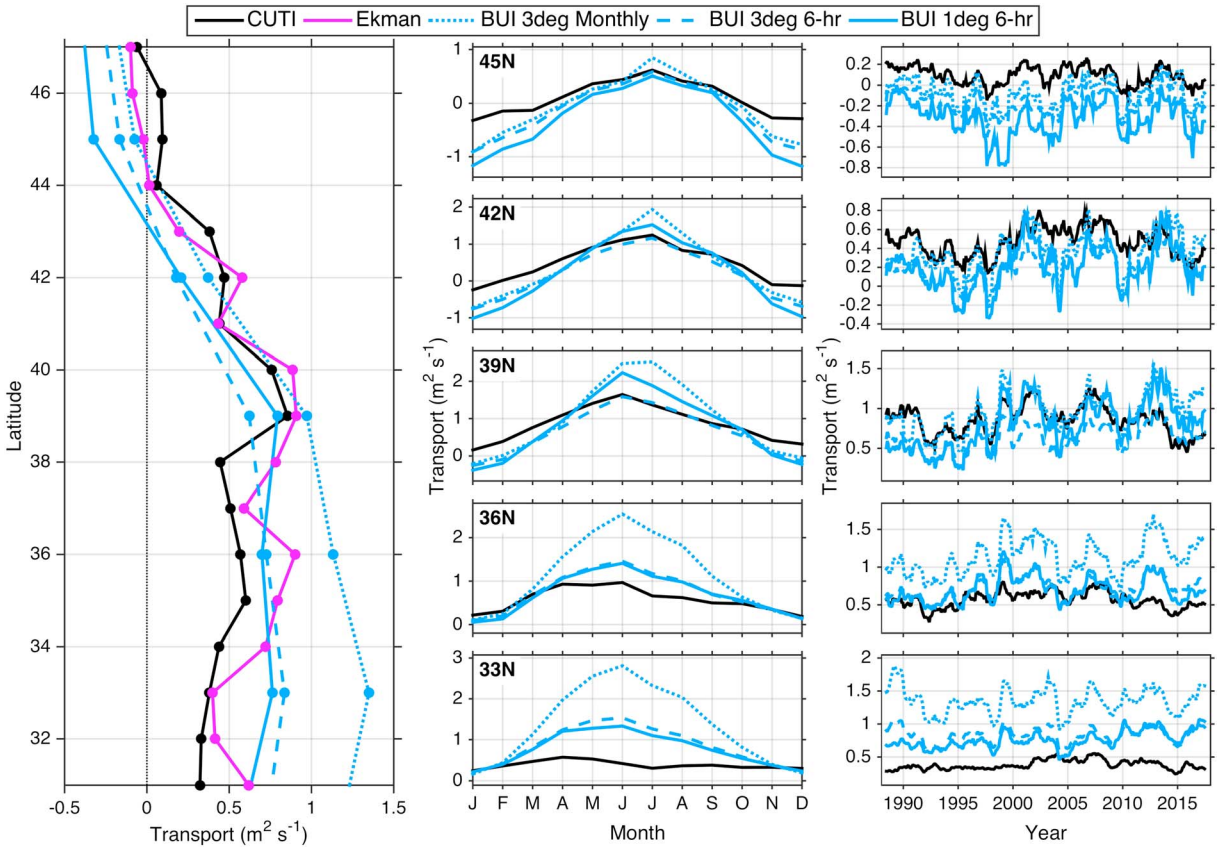

Figure 8. (left) Long-term mean, (middle) seasonal climatology, and (right) interannual variability (12-month running mean) of CUTI and multiple versions of the Bakun Index (BUI), plotted against latitude (left panel) or at select latitudes (middle and right panels). The long-term mean Ekman transport component of CUTI is also plotted for comparison. Indices are shown for 1988–2017. Note scale differences on y-axes of middle and right panels. CUTI = Coastal Upwelling Transport Index.

band used for CUTI likely contributes to the discrepancy as well (Figure 2). At latitudes from 31 to 33°N, CUTI captures ~50–80% of the mean upwelling that occurs within 400 km of the coast, though upwelling farther offshore than CUTI's 75-km integration distance does not produce a response in primary production like that near the coast. At latitudes north of 33°N, >90% of upwelling occurs within 75 km of the coast.

Correlations between CUTI and Bakun Indices are relatively high ($r \cong 0.8–0.9$) at latitudes ≥39°N but deteriorate farther south ($r \cong 0.7–0.8$ at 36°N and 0.4–0.5 at 33°N), and anomaly correlations (monthly climatology removed) follow a similar pattern but with lower values ($r \cong 0.7–0.8$ at latitudes ≥39°N, $r \cong 0.3–0.6$ for 33–36°N; Figure 9). At the southern locations, particularly in the Southern California Bight, Bakun noted the shortcomings of his index at the outset, stating that "the southern California coastal mountain range causes a discontinuity in this pressure gradient such that the gradient actually in equilibrium with the geostrophic wind may be less than that used in the computations. This leads to an overestimation of the geostrophic wind that in turn leads to an overestimation of the upwelling index" (Bakun, 1973). Bakun acknowledged this problem and advised against comparison of his index between locations, and we find that not only the magnitude of upwelling but also its variability is poorly represented off central and southern California (Figure 9).

6. Comparing CUTI and BEUTI

Variability in nitrate availability is not independent from vertical transport; all else being equal, stronger transport draws deeper, more nitrate-rich water to the base of the mixed layer (Jacox & Edwards, 2011). Thus, vertical transport (CUTI) and vertical nitrate flux (BEUTI) are positively correlated (Figure 10) for two reasons: (i) CUTI is positively correlated with subsurface nitrate concentration, and (ii) CUTI is one of the two factors (the other being nitrate concentration) that dictate BEUTI. Since CUTI impacts BEUTI both directly and through the nitrate concentration, the relationship between BEUTI and CUTI is nonlinear (Figure 11).

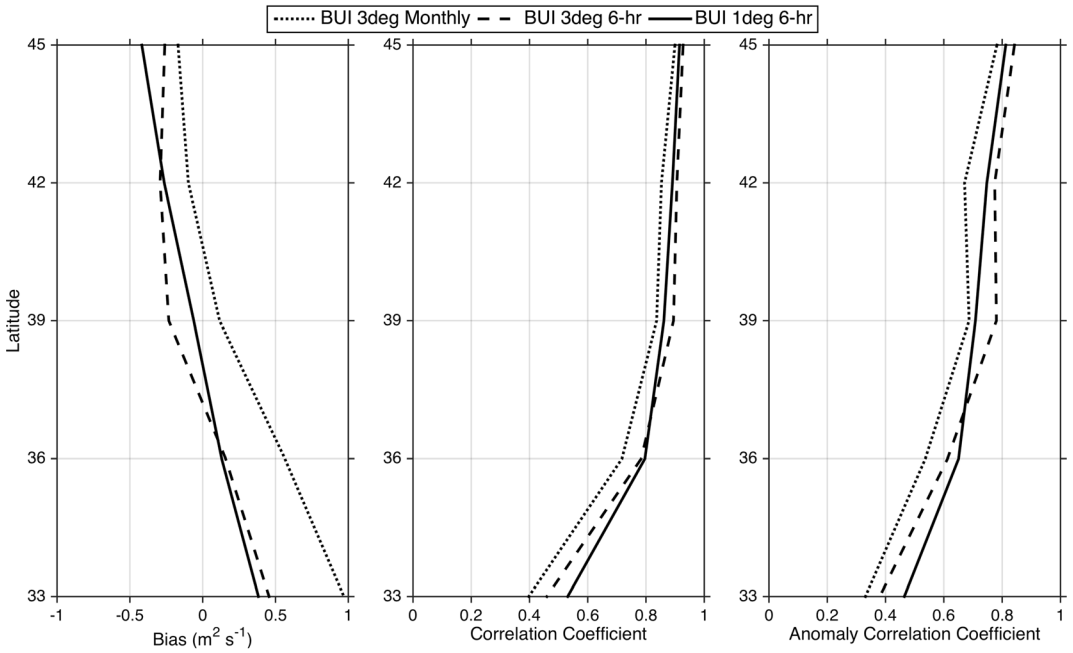

Figure 9. (left) Bias, (middle) correlation coefficient, and (right) anomaly correlation coefficient for multiple versions of the Bakun Index (BUI) relative to the Coastal Upwelling Transport Index, calculated for the period 1988–2017 and plotted against latitude. Correlations were calculated on monthly mean indices to enable comparisons with all three versions of the Bakun Index. For anomaly correlations, the 1988–2017 monthly mean climatology was removed from each index. All correlations are significant above the 99% confidence level.

Nonetheless, scatter in the relationship between CUTI and BEUTI (Figure 11) indicates that subsurface nitrate concentrations exhibit considerable variability that is unrelated to the local vertical transport. On interannual timescales, disconnection between CUTI and BEUTI can be driven by mechanisms including anomalous alongshore advection and coastal trapped wave propagation, which can alter the water column structure independent of the local wind forcing (e.g., Chavez et al., 2002; Jacox, Bograd, et al., 2015; Lynn & Bograd, 2002). A clear example is the juxtaposition of the 1998 and 1999 upwelling seasons, in which remote ocean forcing associated with the 1997–1998 El Niño and the 1998–1999 La Niña dramatically altered nitrate availability along the U.S. West Coast (Bograd & Lynn, 2001; Frischknecht et al., 2017). On seasonal timescales, BEUTI is also influenced by changes in MLD (Figure 7), and on shorter timescales decorrelation of CUTI and BEUTI may also result from lags in the system. For example, a response in BEUTI may lag CUTI as source waters respond to the onset of seasonal upwelling. This effect was particularly pronounced in the delayed upwelling season of 2005, where the spring transition in the northern CCS occurred approximately a month and a half later than the climatological date, but the injection of nutrients into the surface mixed layer and the subsequent phytoplankton response lagged the spring transition by an additional month (Jacox et al., 2016; Kosro et al., 2006).

The relative contributions of CUTI and subsurface nitrate concentration to BEUTI can be explored by looking at how BEUTI relates to each of its two constituents individually (Figure 11). On monthly timescales during the portion of the year most favorable to upwelling (March–September), BEUTI is more strongly correlated with CUTI (r^2 = 0.65) than with nitrate concentration (r^2 = 0.07) in the northern CCS, while in the southern CCS the opposite is true: BEUTI is more strongly correlated with nitrate concentration (r^2 = 0.74) than with CUTI (r^2 = 0.47). In the central CCS, correlations of BEUTI with CUTI and nitrate concentration are similar (r^2 = 0.70 and 0.61, respectively). These latitudinal patterns in CUTI-BEUTI correlation hold across timescales from months to long-term means (Figures 10 and 11) and are consistent with the notion that the southern portion of the CCS is influenced more strongly by remote oceanic forcing that modulates nitrate fluxes through changes in the water column structure (e.g., deepening/shoaling of the nitracline), while the northern CCS is driven more by local atmospheric forcing that alters nitrate flux through changes in the strength of upwelling/downwelling (Frischknecht et al., 2015).

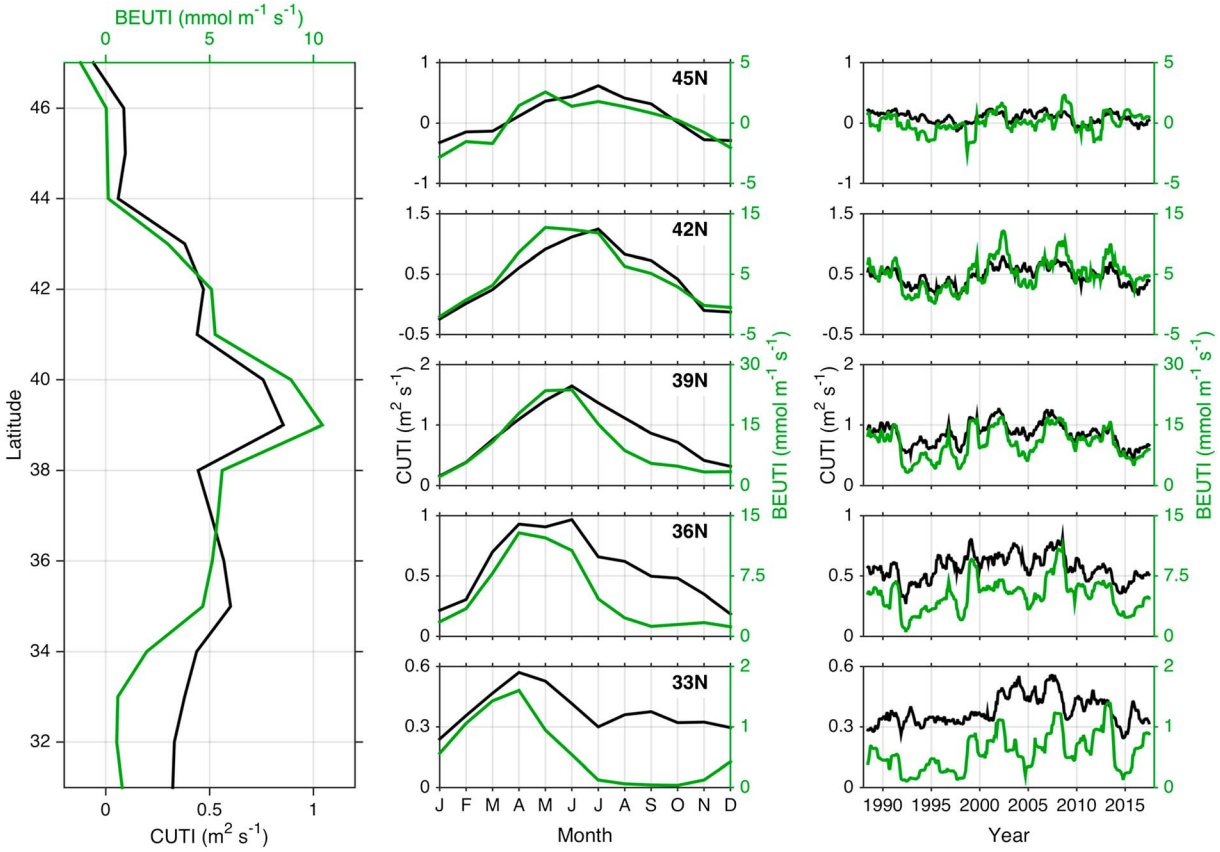

Figure 10. (left) Long-term mean, (middle) seasonal climatology, and (right) interannual variability (12-month running mean) of CUTI and BEUTI, plotted against latitude (left panel) or at select latitudes (middle and right panels). Indices are shown for 1988–2017. Note scale differences on *y*-axes of middle and right panels. CUTI = Coastal Upwelling Transport Index; BEUTI = Biologically Effective Upwelling Transport Index.

7. Discussion

In this paper, we have introduced two new upwelling indices—CUTI and BEUTI—that provide daily estimates of vertical transport and vertical nitrate flux, respectively, along the U.S. West Coast. We prefaced the introduction of CUTI and BEUTI with a review of Ekman dynamics and the widely used Bakun Index so that the theory, data, models, and assumptions that underlie each of these indices are clear. CUTI and BEUTI improve upon the Bakun Index by (i) leveraging advances in ocean and atmospheric observations and models, (ii) including a more complete description of the coastal ocean circulation, and (iii) estimating changes in the nitrate content of upwelled waters. Like all indices, CUTI and BEUTI should be used with an understanding of the assumptions and caveats involved in their construction and application, and we expand on those below.

7.1. Additional Considerations for Using CUTI and BEUTI

Idealized Ekman dynamics set up within several hours after the onset of wind forcing at midlatitudes. However, Chereskin (1995), using vertical velocity profiles obtained over several months of continuous spring/summer observations, found that the wind-driven flow off the northern California coast was in Ekman balance "on timescales as short as a few days," with good agreement on timescales of 3–5 days and occasional periods when the Ekman balance prevailed in daily averages. Thus, while we provide CUTI and BEUTI at daily frequency (and Bakun Indices are provided every 6 hr), observations suggest they may be more applicable on timescales of several days or more.

The upwelling estimates discussed here do not describe the cross-shore structure of upwelling, as they are integrated over a fixed cross-shore region. Within this region, the same net upwelling can theoretically be generated by multiple different wind profiles (e.g., in a 2-D simplification, where two cases have the same

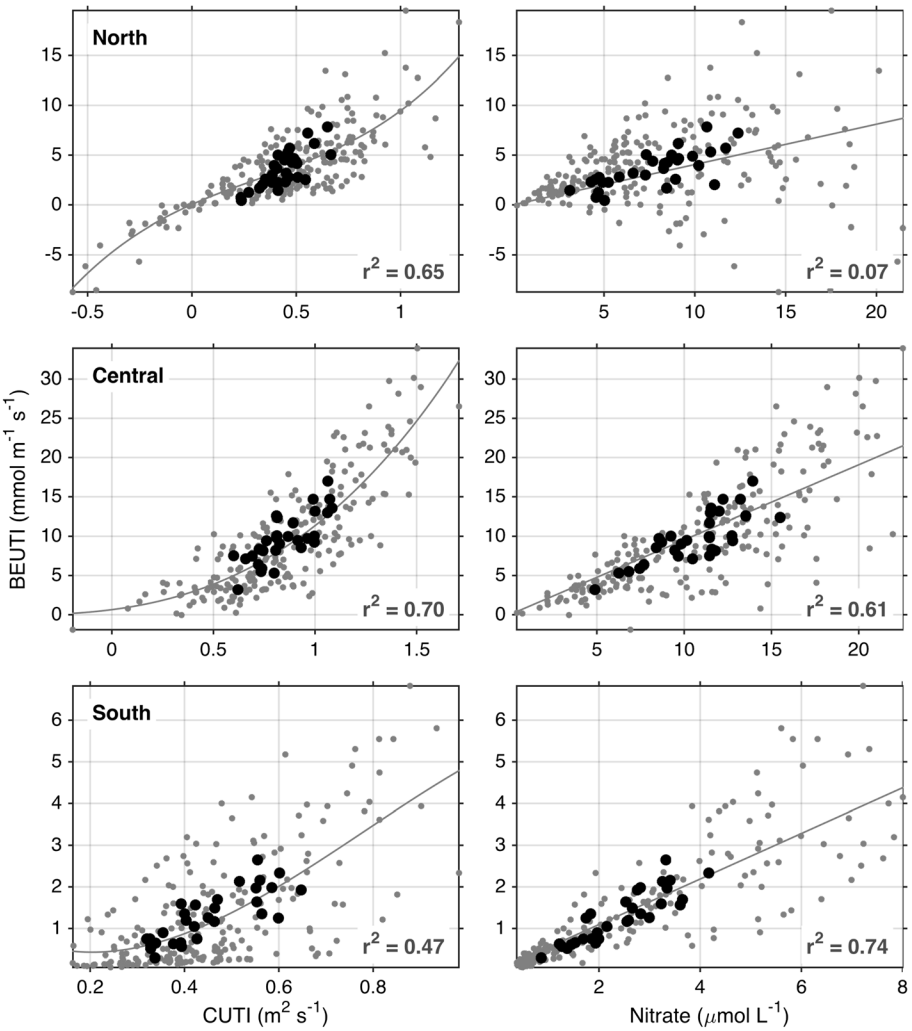

Figure 11. BEUTI is plotted against its two components, (left) CUTI and (right) nitrate concentration at the base of the mixed layer. Data are constrained to the upwelling season (March–September) and are averaged monthly (small gray dots) and annually (large black dots). North, central, and southern California Current System values represent averages of 1° latitude indices over 41–47°N, 35–40°N, and 31–34°N, respectively. In each panel, the gray line indicates either a (left) cubic or (right) linear fit to the monthly data, and the coefficient of determination is displayed for that fit. BEUTI = Biologically Effective Upwelling Transport Index; CUTI = Coastal Upwelling Transport Index.

offshore equatorward wind stress but one has a narrow band of steep coastal wind drop-off while the other has a wider band of gradual wind drop-off). These contrasting wind profiles can have very different implications for the physical and biogeochemical dynamics (Capet et al., 2004; Jacox & Edwards, 2012; Renault, Deutsch, et al., 2016), but they are not explicitly represented in the Bakun Index, CUTI, or BEUTI. However, these effects are implicit in BEUTI to a degree, as its nitrate component reflects modification of the subsurface density structure by the spatially resolved wind field.

BEUTI is an estimate of nitrate flux, which is the product of vertical transport (CUTI) and subsurface nitrate concentration. However, biological effects have been shown to depend on independent influences of upwelling and nutrient availability. For example, Jacox et al. (2016) found that chlorophyll biomass off the U.S. West Coast is maximized at moderate wind stress values (consistent with previous studies by Botsford et al., 2003, and others) but also that for a given wind stress the chlorophyll biomass is strongly modified by variability in the subsurface nitrate concentration. A single value of BEUTI can represent quite different wind/nitrate conditions (e.g., one case with strong upwelling of nitrate-poor water and another case with weak upwelling of nitrate-rich water), which may have very different implications for the ecosystem. If exploration of these types

of effects is of interest, one can divide BEUTI by CUTI to recover an estimate of subsurface nitrate concentration.

During downwelling conditions, negative values of BEUTI are reported. Particularly in the northern CCS, negative BEUTI values can be relatively large since downwelling conditions tend to occur in the winter when nitrate concentrations at the base of the mixed layer are also high due to deep mixing. Users may choose to set negative BEUTI values to zero if only upward nitrate fluxes are deemed relevant (e.g., Schroeder et al., 2013), for example, under the assumption that all nutrients entering the surface mixed layer are biologically available.

BEUTI relies on temperature and latitude as proxies for nitrate; therefore, uncertainty in nitrate estimates can arise from uncertainty in either the modeled temperature or the latitude-temperature-nitrate relationship. In a previous study, Jacox, Bograd, et al., (2015) found strong correspondence over several decades between observed subsurface nitrate concentrations and those derived from CCSRA31, and the statistical relationship used herein to estimate nitrate is very robust in the historical data, capturing over 90% of the observed variance in the CCS (Figure 6). Nonetheless, the latitude-temperature-nitrate relationship is subject to concerns of nonstationarity related to interannual variability (Kim & Miller, 2007) and longer-term trends (Bograd et al., 2015; Rykaczewski & Dunne, 2010) and should be periodically validated/updated based on available in situ observations.

Finally, while CUTI and BEUTI are designed to aid understanding of bottom-up forcing in the CCS, a number of additional factors not captured by these indices can impact the relationships between upwelling and biological responses. Examples include top-down forcing, variable light levels, freshwater input, and availability of nutrients other than nitrate, particularly micronutrients like iron (Hutchins et al., 1998).

7.2. Creating Similar Indices for Other Regions

A key strength of the Bakun Index is that in theory it can be calculated for any coastline in the global ocean. In regions where the oceanographic model output needed to calculate CUTI or BEUTI are unavailable, SLP (or better yet surface wind stress) from atmospheric reanalyses can be used to estimate upwelling. We suggest calculating Ekman transport as we have here, by integrating along all boundaries of the region of interest rather than rotating winds and estimating offshore transport. Integration around the region of interest eliminates the need for estimating the coastline orientation, ensures that Ekman transport/pumping associated with alongshore and cross-shore variations in the wind are captured, and enables more accurate closure of the transport budget. In regions where high-resolution oceanographic analyses are available, the methodology presented here can be applied to create similar indices.

As mentioned earlier, an index like CUTI that incorporates both the Ekman and geostrophic transports can in principle be derived for any region with reasonable estimates of surface wind stress and alongshore SSH gradients or geostrophic currents (e.g., Marchesiello & Estrade, 2010, Rossi et al., 2013). However, developing such an index from surface (e.g., remote sensing) observations alone introduces additional assumptions and uncertainties with respect to the cross-shore geostrophic transport. First, the convergence of cross-shore geostrophic transport at the coast is dictated by the alongshore pressure gradient near shore (within tens of kilometers of the coast). Unfortunately, at present satellite SSH measurements are unreliable within 25–50 km of the coast, though blended satellite/tide gauge products offer promise for addressing this coastal gap (Saraceno et al., 2008). Second, calculation of the relevant cross-shore geostrophic transport requires an estimate of the depth over which geostrophic flow interacts constructively or destructively with Ekman transport. This depth (in our case the MLD) cannot be readily obtained from remote sensing platforms; one could instead use climatological MLD values obtained from observations or generate MLD estimates by making assumptions about the vertical mixing (e.g., Rossi et al., 2013), though both of these approaches introduce additional uncertainty.

Building BEUTI based on surface data is more difficult, as it seeks to describe subsurface water column structure that can vary independent of the surface forcing. However, we present two options here. The first is to combine CUTI with climatological data on MLD and subsurface nutrient concentrations (see Messié et al., 2009). While this approach omits important interannual variability in the subsurface nitrate field, it would allow inclusion of the considerable seasonal and latitudinal nitrate variability (left and middle panels of Figure 7). Alternatively, one could derive a proxy for nitrate at the base of the mixed layer by (i) defining

temperature at the base of the mixed layer as a specified departure from the sea surface temperature and (ii) using that temperature to estimate nitrate from an empirical relationship (e.g., Figure 6). This approach allows for a more dynamic estimate of subsurface nitrate concentrations but introduces uncertainty by estimating MLD from temperature alone rather than from density or other metrics of vertical stratification.

8. Conclusion

We have described here two new upwelling indices—one (CUTI) that is comparable to the Bakun Index in that it estimates vertical volume transport, and another (BEUTI) that estimates vertical nitrate flux as potentially a better indicator of bottom-up influences on phytoplankton and consequently on higher trophic levels. Relative to existing upwelling indices, the new indices more accurately integrate the relevant atmospheric and oceanographic dynamics, primarily by leveraging technological advances realized in recent decades. For applications where indices of upwelling or nitrate flux are desired, and for which the study area and time period are covered by the indices presented here, we believe CUTI and BEUTI represent significant improvement over what has previously been available and we hope they prove to be beneficial in understanding wind forcing of the CCS.

Acknowledgments
We are grateful to L. DeWitt for discussions on the history of the Bakun Index and its iterations; to L. DeWitt and H. Welch for support in serving the new indices; to F. Schwing, T. Garfield and two anonymous reviewers for suggestions that guided improvements to the manuscript; and to A. Moore for his efforts developing the historical ocean reanalyses and for helpful discussions in the early stages of this work. All upwelling indices, including CUTI, BEUTI, and multiple versions of the Bakun Index, are available for viewing and download at oceanview.pfeg.noaa.gov/products/upwelling and www.mjacox.com/upwelling-indices. ROMS reanalyses can be accessed via the UCSC ocean modeling group's webpage (http://oceanmodeling.ucsc.edu).

References

Allen, J. S., & Smith, R. L. (1981). On the dynamics of wind-driven shelf currents. *Philosophical Transactions. Royal Society of London*, *A302*, 617–634.

Bakun, A. (1973). Coastal upwelling indices, West Coast of North America, 1946–71. US Department of Commerce, National Oceanic and Atmospheric Administration, National Marine Fisheries Service.

Bakun, A. (1975). Daily and weekly upwelling indices, West Coast of North America. NOAA Tech. Rpt, 16.

Barton, E. D., Huyer, A., & Smith, R. L. (1977). Temporal variation observed in the hydrographic regime near Cabo Corveiro in the northwest African upwelling region, February to April 1974. *Deep Sea Research*, *24*(1), 7–23. https://doi.org/10.1016/0146-6291(77)90537-9

Bograd, S. J., Hazen, E. L., Maxwell, S., Leising, A. W., Bailey, H., & Brodeur, R. (2016). Offshore ecosystems. In H. Mooney & E. Zavaleta (Eds.), *Ecosystems of California—A source book* (pp. 287–309). Oakland, CA: University of California Press.

Bograd, S. J., & Lynn, R. J. (2001). Physical-biological coupling in the California Current during the 1997–99 El Niño-La Niña cycle. *Geophysical Research Letters*, *28*(2), 275–278.

Bograd, S. J., Pozo Buil, M., Di Lorenzo, E., Castro, C. G., Schroeder, I. D., Goericke, R., et al. (2015). Changes in source waters to the Southern California Bight. *Deep Sea Research, Part II*, *112*, 42–52. https://doi.org/10.1016/j.dsr2.2014.04.009

Botsford, L. W., Lawrence, C. A., Dever, E. P., Hastings, A., & Largier, J. (2003). Wind strength and biological productivity in upwelling systems: An idealized study. *Fisheries Oceanography*, *12*(4–5), 245–259. https://doi.org/10.1046/j.1365-2419.2003.00265.x

Brodeur, R. D., & Ware, D. M. (1992). Long-term variability in zooplankton biomass in the subarctic Pacific Ocean. *Fisheries Oceanography*, *1*(1), 32–38. https://doi.org/10.1111/j.1365-2419.1992.tb00023.x

Brown, W. S., Irish, J. D., & Winant, C. D. (1987). A description of subtidal pressure field observations on the northern California shelf during the Coastal Ocean Dynamics Experiment. *Journal of Geophysical Research*, *92*(C2), 1605–1636. https://doi.org/10.1029/JC092iC02p01605

Capet, X. J., Marchesiello, P., & McWilliams, J. C. (2004). Upwelling response to coastal wind profiles. *Geophysical Research Letters*, *31*, L13311. https://doi.org/10.1029/2004GL020123

Chavez, F., Pennington, J., Castro, C., Ryan, J., Michisaki, R., Schlining, B., et al. (2002). Biological and chemical consequences of the 1997–1998 El Niño in central California waters. *Progress in Oceanography*, *54*(1–4), 205–232. https://doi.org/10.1016/S0079-6611(02)00050-2

Chereskin, T. K. (1995). Direct evidence for an Ekman balance in the California Current. *Journal of Geophysical Research*, *100*(C9), 18,261–18,269. https://doi.org/10.1029/95JC02182

Chhak, K., & Di Lorenzo, E. (2007). Decadal variations in the California Current upwelling cells. *Geophysical Research Letters*, *34*, L14604. https://doi.org/10.1029/2007GL030203

Colas, F., Capet, X., McWilliams, J. C., & Shchepetkin, A. (2008). 1997–1998 El Niño off Peru: A numerical study. *Progress in Oceanography*, *79*(2-4), 138–155. https://doi.org/10.1016/j.pocean.2008.10.015

Connolly, T. P., Hickey, B. M., Shulman, I., & Thomson, R. E. (2014). Coastal trapped waves, alongshore pressure gradients, and the California undercurrent. *Journal of Physical Oceanography*, *44*(1), 319–342. https://doi.org/10.1175/JPO-D-13-095.1

Croll, D. A., Marinovic, B., Benson, S., Chavez, F. P., Black, N., Ternullo, R., & Tershy, B. R. (2005). From wind to whales: Trophic links in a coastal upwelling system. *Marine Ecology Progress Series*, *289*, 117–130. https://doi.org/10.3354/meps289117

Dever, E. P., Dorman, C. E., & Largier, J. L. (2006). Surface boundary-layer variability off northern California, USA, during upwelling. *Deep Sea Research Part II: Topical Studies in Oceanography*, *53*(25–26), 2887–2905. https://doi.org/10.1016/j.dsr2.2006.09.001

Di Lorenzo, E., Schneider, N., Cobb, K. M., Franks, P. J. S., Chhak, K., Miller, A. J., et al. (2008). North Pacific gyre oscillation links ocean climate and ecosystem change. *Geophysical Research Letters*, *35*, L08607. https://doi.org/10.1029/2007GL032838

Ekman, V. W. (1905). On the influence of the earth's rotation on ocean-currents. *Arkiv foer Matematik, Astronomi, och Fysik*, *2*(11), 1–53.

Enfield, D. B., & Allen, J. S. (1980). On the structure and dynamics of monthly mean sea level anomalies along the Pacific coast of North and South America. *Journal of Physical Oceanography*, *10*(4), 557–578. https://doi.org/10.1175/1520-0485(1980)010<0557:OTSADO>2.0.CO;2

Estrade, P., Marchesiello, P., Colin de Verdiere, A., & Roy, C. (2008). Cross-shelf structure of coastal upwelling: A two-dimensional expansion of Ekman's theory and a mechanism for innershelf upwelling shut down. *Journal of Marine Research*, *66*(5), 589–616. https://doi.org/10.1357/002224008787536790

Fairall, C. W., Bradley, E. F., Godfrey, J. S., Wick, G. A., Edson, J. B., & Young, G. S. (1996). Cool-skin and warm-layer effects on the sea surface temperature. *Journal of Geophysical Research*, *101*(C1), 1295–1308. https://doi.org/10.1029/95JC03190

Fairall, C. W., Bradley, E. F., Rogers, D. P., Edson, J. B., & Young, G. S. (1996). Bulk parameterization of air-sea fluxes for Tropical Ocean-Global Atmosphere Coupled-Ocean Atmosphere Response Experiment. *Journal of Geophysical Research*, *101*(C2), 3747–3764. https://doi.org/10.1029/95JC03205

Fiechter, J., Curchitser, E. N., Edwards, C. A., Chai, F., Goebel, N. L., & Chavez, F. P. (2014). Air-sea CO2 fluxes in the California Current: Impacts of model resolution and coastal topography. *Global Biogeochemical Cycles*, *28*, 371–385. https://doi.org/10.1002/2013GB004683

Frischknecht, M., Münnich, M., & Gruber, N. (2015). Remote versus local influence of ENSO on the California Current system. *Journal of Geophysical Research: Oceans*, *120*, 1353–1374. https://doi.org/10.1002/2014JC010531

Frischknecht, M., Münnich, M., & Gruber, N. (2017). Local atmospheric forcing driving an unexpected California Current system response during the 2015-2016 El Niño. *Geophysical Research Letters*, *44*, 304–311. https://doi.org/10.1002/2016GL071316

Hickey, B. M. (1984). The fluctuating longshore pressure gradient on the Pacific Northwest shelf: A dynamical analysis. *Journal of Physical Oceanography*, *14*(2), 276–293. https://doi.org/10.1175/1520-0485(1984)014<0276:TFLPGO>2.0.CO;2

Hutchins, D. A., DiTullio, G. R., Zhang, Y., & Bruland, K. W. (1998). An iron limitation mosaic in the California upwelling regime. *Limnology and Oceanography*, *43*(6), 1037–1054. https://doi.org/10.4319/lo.1998.43.6.1037

Jacox, M. G., Bograd, S. J., Hazen, E. L., & Fiechter, J. (2015). Sensitivity of the California Current nutrient supply to wind, heat, and remote ocean forcing. *Geophysical Research Letters*, *42*, 5950–5957. https://doi.org/10.1002/2015GL065147

Jacox, M. G., & Edwards, C. A. (2011). Effects of stratification and shelf slope on nutrient supply in coastal upwelling regions. *Journal of Geophysical Research*, *116*, C03019. https://doi.org/10.1029/2010JC006547

Jacox, M. G., & Edwards, C. A. (2012). Upwelling source depth in the presence of nearshore wind stress curl. *Journal of Geophysical Research*, *117*, C05008. https://doi.org/10.1029/2011JC007856

Jacox, M. G., Fiechter, J., Moore, A. M., & Edwards, C. A. (2015). ENSO and the California Current coastal upwelling response. *Journal of Geophysical Research: Oceans*, *120*, 1691–1702. https://doi.org/10.1002/2014JC010650

Jacox, M. G., Hazen, E. L., & Bograd, S. J. (2016). Optimal environmental conditions and anomalous ecosystem responses: Constraining bottom-up controls of phytoplankton biomass in the California Current system. *Scientific Reports*, *6*(1), 27612. https://doi.org/10.1038/srep27612

Jacox, M. G., Moore, A. M., Edwards, C. A., & Fiechter, J. (2014). Spatially resolved upwelling in the California Current system and its connections to climate variability. *Geophysical Research Letters*, *41*, 3189–3196. https://doi.org/10.1002/2014GL059589

Kara, A. B., Rochford, P. A., & Hurlburt, H. E. (2000). An optimal definition for ocean mixed layer depth. *Journal of Geophysical Research*, *105*(C7), 16,803–16,821. https://doi.org/10.1029/2000JC900072

Kim, H. J., & Miller, A. J. (2007). Did the thermocline deepen in the California Current after the 1976/77 climate regime shift? *Journal of Physical Oceanography*, *37*(6), 1733–1739. https://doi.org/10.1175/JPO3058.1

Koračin, D., & Dorman, C. E. (2001). Marine atmospheric boundary layer divergence and clouds along California in June 1996. *Monthly Weather Review*, *129*(8), 2040–2056. https://doi.org/10.1175/1520-0493(2001)129<2040:MABLDA>2.0.CO;2

Kosro, P. M., Peterson, W. T., Hickey, B. M., Shearman, R. K., & Pierce, S. D. (2006). Physical versus biological spring transition: 2005. *Geophysical Research Letters*, *33*, L22S03. https://doi.org/10.1029/2006GL027072

Large, W., & Pond, S. (1981). Open Ocean momentum flux measurements in moderate to strong winds. *Journal of Physical Oceanography*, *11*(3), 324–336. https://doi.org/10.1175/1520-0485(1981)011<0324:OOMFMI>2.0.CO;2

Lentz, S. J. (1994). Current dynamics over the northern California inner shelf. *Journal of Physical Oceanography*, *24*(12), 2461–2478. https://doi.org/10.1175/1520-0485(1994)024<2461:CDOTNC>2.0.CO;2

Lentz, S. J., & Chapman, D. C. (2004). The importance of nonlinear cross-shelf momentum flux during wind-driven coastal upwelling. *Journal of Physical Oceanography*, *34*(11), 2444–2457. https://doi.org/10.1175/JPO2644.1

Liu, W. T., Katsaros, K. B., & Businger, J. A. (1979). Bulk parameterization of the air-sea exchange of heat and water vapor including the molecular constraints at the interface. *Journal of the Atmospheric Sciences*, *36*(9), 1722–1735. https://doi.org/10.1175/1520-0469(1979)036<1722:BPOASE>2.0.CO;2

Lynn, R., & Bograd, S. (2002). Dynamic evolution of the 1997–1999 El Niño-La Niña cycle in the southern California Current system. *Progress in Oceanography*, *54*(1–4), 59–75. https://doi.org/10.1016/S0079-6611(02)00043-5

Marchesiello, P., & Estrade, P. (2010). Upwelling limitation by onshore geostrophic flow. *Journal of Marine Research*, *68*(1), 37–62. https://doi.org/10.1357/002224010793079004

Messié, M., Ledesma, J., Kolber, D. D., Michisaki, R. P., Foley, D. G., & Chavez, F. P. (2009). Potential new production estimates in four eastern boundary upwelling ecosystems. *Progress in Oceanography*, *83*(1–4), 151–158.

Moore, A. M., Edwards, C. A., Fiechter, J., Drake, P., Arango, H. G., Neveu, E., et al. (2013). A 4D-Var analysis system for the California Current: A prototype for an operational regional ocean data assimilation system. In L. Xu & S. Park (Eds.), *Data assimilation for atmospheric, oceanic and hydrological applications* (Vol. II, pp. 345–366). Berlin: Springer.

Nansen, F. (1902). The oceanography of the north polar basin. In *Norwegian North Pole Expedition. 1893–1896, Scientific Results* (Vol. 3, pp. 357–386). Toronto, Ontario: Longmans, Green.

Neveu, E., Moore, A. M., Edwards, C. A., Fiechter, J., Drake, P., Jacox, M. G., & Nuss, E. (2016). A historical analysis of the California Current using ROMS 4D-Var. Part I: System configuration and diagnostics. *Ocean Modelling*, *99*, 133–151. https://doi.org/10.1016/j.ocemod.2015.11.012

Oerder, V., Colas, F., Echevin, V., Codron, F., Tam, J., & Belmadani, A. (2015). Peru-Chile upwelling dynamics under climate change. *Journal of Geophysical Research: Oceans*, *120*, 1152–1172. https://doi.org/10.1002/2014JC010299

Parrish, R. H., Nelson, C. S., & Bakun, A. (1981). Transport mechanisms and reproductive success of fishes in the California Current. *Biological Oceanography*, *1*(2), 175–203.

Pickett, M. H., & Paduan, J. D. (2003). Ekman transport and pumping in the California Current based on the U.S. Navy's high-resolution atmospheric model (COAMPS). *Journal of Geophysical Research*, *108*(C10), 3327. https://doi.org/10.1029/2003JC001902

Reiter, J., Stinson, N. L., & Le Boeuf, B. J. (1978). Northern elephant seal development: The transition from weaning to nutritional independence. *Behavioral Ecology and Sociobiology*, *3*(4), 337–367. https://doi.org/10.1007/BF00303199

Renault, L., Deutsch, C., McWilliams, J. C., Frenzel, H., Liang, J. H., & Colas, F. (2016). Partial decoupling of primary productivity from upwelling in the California Current system. *Nature Geoscience*, *9*(7), 505–508. https://doi.org/10.1038/ngeo2722

Renault, L., Hall, A., & McWilliams, J. C. (2016). Orographic shaping of US West Coast wind profiles during the upwelling season. *Climate Dynamics*, *46*(1–2), 273–289. https://doi.org/10.1007/s00382-015-2583-4

Rossi, V., Feng, M., Pattiaratchi, C., Roughan, M., & Waite, A. M. (2013). On the factors influencing the development of sporadic upwelling in the Leeuwin Current system. *Journal of Geophysical Research: Oceans*, *118*, 3608–3621. https://doi.org/10.1002/jgrc.20242

Rykaczewski, R. R., & Checkley, D. M. (2008). Influence of ocean winds on the pelagic ecosystem in upwelling regions. *Proceedings of the National Academy of Sciences*, *105*(6), 1965–1970. https://doi.org/10.1073/pnas.0711777105

Rykaczewski, R. R., & Dunne, J. P. (2010). Enhanced nutrient supply to the California Current ecosystem with global warming and increased stratification in an earth system model. *Geophysical Research Letters*, *37*, L21606. https://doi.org/10.1029/2010GL045019

Rykaczewski, R. R., Dunne, J. P., Sydeman, W. J., García-Reyes, M., Black, B. A., & Bograd, S. J. (2015). Poleward displacement of coastal upwelling-favorable winds in the ocean's eastern boundary currents through the 21st century. *Geophysical Research Letters*, *42*, 6424–6431. https://doi.org/10.1002/2015GL064694

Saraceno, M., Strub, P. T., & Kosro, P. M. (2008). Estimates of sea surface height and near-surface alongshore coastal currents from combinations of altimeters and tide gauges. *Journal of Geophysical Research*, *113*, C11013. https://doi.org/10.1029/2008JC004756

Schroeder, I. D., Black, B. A., Sydeman, W. J., Bograd, S. J., Hazen, E. L., Santora, J. A., & Wells, B. K. (2013). The North Pacific High and wintertime pre-conditioning of California Current productivity. *Geophysical Research Letters*, *40*, 541–546. https://doi.org/10.1002/grl.50100

Schwing, F. B., Murphree, T., & Green, P. M. (2002). The Northern Oscillation Index (NOI): A new climate index for the Northeast Pacific. *Progress in Oceanography*, *53*(2–4), 115–139. https://doi.org/10.1016/S0079-6611(02)00027-7

Schwing, F. B., O'Farrell, M., Steger, J. M., & Baltz, K. (1996). Coastal Upwelling indices West Coast of North America. NOAA Tech. Rep., NMFS SWFSC, 231 (144 pp.).

Small, L. F., & Menzies, D. W. (1981). Patterns of primary productivity and biomass in a coastal upwelling region. *Deep Sea research Part A. Oceanographic Research Papers*, *28*(2), 123–149. https://doi.org/10.1016/0198-0149(81)90086-8

Trenberth, K. E., Large, W. G., & Olson, J. G. (1990). The mean annual cycle in global ocean wind stress. *Journal of Physical Oceanography*, *20*(11), 1742–1760. https://doi.org/10.1175/1520-0485(1990)020<1742:TMACIG>2.0.CO;2

Verdy, A., Mazloff, M. R., Cornuelle, B. D., & Kim, S. Y. (2014). Wind-driven sea level variability on the California coast: An adjoint sensitivity analysis. *Journal of Physical Oceanography*, *44*(1), 297–318. https://doi.org/10.1175/JPO-D-13-018.1